Unveiling the plating-stripping mechanism in aluminum batteries with imidazolium-based electrolytes

A hierarchical model based on experiments and ab initio simulations

Appiah, Williams Agyei; Stark, Anna; Lysgaard, Steen; Busk, Jonas; Jankowski, Piotr; Chang, Jin Hyun; Bhowmik, Arghya; Gollas, Bernhard; Garcia-Lastra, Juan Maria

Published in:
Chemical Engineering Journal

Link to article, DOI:
10.1016/j.cej.2023.144995

Publication date:
2023

Document Version
Publisher's PDF, also known as Version of record

Chemical Engineering Journal 472 (2023) 144995

Contents lists available at ScienceDirect

Chemical Engineering Journal

journal homepage: www.elsevier.com/locate/cej

Unveiling the plating-stripping mechanism in aluminum batteries with imidazolium-based electrolytes: A hierarchical model based on experiments and ab initio simulations

Williams Agyei Appiah [a,*], Anna Stark [b], Steen Lysgaard [a], Jonas Busk [a], Piotr Jankowski [a,c], Jin Hyun Chang [a], Arghya Bhowmik [a], Bernhard Gollas [b], Juan Maria Garcia-Lastra [a,*]

[a] Department of Energy Conversion and Storage, Technical University of Denmark, Kgs. Lyngby, 2800 Denmark
[b] Institute for Chemistry and Technology of Materials, Graz University of Technology, Graz A-8010, Austria
[c] Faculty of Chemistry, Warsaw University of Technology, Warsaw 00-661, Poland

ARTICLE INFO

Keywords:
Aluminum batteries
Ionic liquid electrolytes
Physics-based model
Sensitivity analysis

ABSTRACT

Aluminum batteries with imidazolium-based electrolytes present a promising avenue toward the post-lithium-ion battery era. A critical bottleneck is the development of reversible aluminum metal anodes, which is hindered by sluggish battery charge–discharge characteristics due to the reversible/irreversible side reactions on the anodic and cathodic sides. The indispensable discernment of the stripping-plating mechanisms at the electrode–electrolyte interface is not well explored due to the complexity of the various reactions occurring at the surface of the aluminum anode. Herein, a high-fidelity physics-based model is coupled with density functional theory to explain the stripping-plating mechanisms that occur on the surface of the aluminum anode at different current densities. Sensitivity analysis is performed on the experimentally validated physics-based model using a machine-learning Gaussian process regression model to identify the most significant parameters for the plating-stripping mechanism of aluminum. The electrodeposition of aluminum is controlled by both diffusion and kinetics and is limited by the kinetics of the electrochemical reactions at a high current density. This work highlights the assurance of combining models at different scales, machine learning algorithms, and experiments to analyze the behavior of complex electrochemical systems.

1. Introduction

Rechargeable aluminum batteries (RABs) with imidazolium-based ionic liquid (IL) electrolytes such as 1-ethyl-3-methylimidazolium chloride (EMIMCl)-$AlCl_3$ are of great interest as aluminum metal negative electrode could deliver a high theoretical and volumetric capacity of 2980 mAh g^{-1} and 8046 mAh cm^{-3}, respectively [1–4], as well as enhanced safety compared to existing lithium-ion batteries (LIBs) [5]. The inability to effectively plate and strip aluminum metal during charge and discharge at practical current densities stems from the presence of a dense and non-conductive oxide film at the surface of the aluminum metal, which leads to poor electrochemical performance and is one of the major factors that hinders the progress to commercialization of RABs [6–9]. Previous work has demonstrated that a suitable concentration of the electroactive Lewis acidic chloroaluminate anion,$Al_2Cl_7^-$, causes slight pitting on the aluminum metal anode during plating, which removes the oxide film and enhances the electrochemical performance [10]. However, the plating-stripping mechanism of RABs involves the formation of other intermediate species ($AlCl_3^-$, $AlCl_2^-$ and $AlCl^-$) [11,12] as well as the other major chloroaluminate anion $AlCl_4^-$. An in-depth understanding of the effects of the oxide layer and the concentration of the electroactive species on the plating-stripping mechanism at different current densities will help accelerate the development of RABs.

The most widely investigated IL for plating and stripping aluminum is the mixture of EMIMCl and $AlCl_3$ with an excess amount of $AlCl_3$ owing to its high ionic conductivity and enhanced thermal and electrochemical stability [13–19]. The major electroactive species responsible for the plating of aluminum from ILs is the easily reducible heptachloroaluminate anion, $Al_2Cl_7^-$ according to reaction (1) [3,20,21], while the prevalent tetrachloroaluminate anion $AlCl_4^-$ in the neutral melts exhibits a more cathodic reduction potential as compared

* Corresponding authors.
E-mail addresses: wagap@dtu.dk (W.A. Appiah), jmgla@dtu.dk (J.M. Garcia-Lastra).

https://doi.org/10.1016/j.cej.2023.144995
Received 14 April 2023; Received in revised form 8 July 2023; Accepted 22 July 2023
Available online 24 July 2023

to the imidazolium cation, $EMIM^+$.

$$4Al_2Cl_7^- + 3e^- \longleftrightarrow^{charge}_{discharge} Al + 7AlCl_4^- \quad (1)$$

However, reaction (1), proceeds with a high activation energy (>400 kJ mol^{-1}), which makes it highly unlikely to occur [11]. Thus it is reasonable to assume three successive one-electron transfers, one of them being the rate-determining step (RDS) [22]. This assumption has been considered in studying the deposition and dissolution of aluminum in various kinds of electrolytes [23–25], including (EMIMCl)-$AlCl_3$ ILs [11,12]. However, during the plating and stripping of aluminum, the concentrations of the major electroactive species and the intermediates at the aluminum metal/electrolyte interface play a critical role in the overpotential generated in the cell, especially at high current densities and hence needs to be considered.

Much effort has been utilized to understand the plating-stripping mechanisms of lithium-ion batteries using electrochemical models [26–29]. However, the application of such a time-effective and efficient method is limited in RABs. Schaltin et al. [17] exploited the origin of reasonable current densities achieved during the electrodeposition of aluminum from chloroaluminate ionic liquids via finite element modeling. Therein, the authors extended reaction (1) to include the kinetics of the reaction between Cl^- and $Al_2Cl_7^-$ to produce $AlCl_4^-$ ($3Cl^- + 3Al_2Cl_7^- \rightarrow 6AlCl_4^-$) and established an auto-solvolysis equilibrium reaction for the three anions ($Al_2Cl_7^- + Cl^- \longleftrightarrow^{k_f}_{k_b} 2AlCl_4^-$). They observed that the calculated current densities strongly depended on the rate constants, k_f and k_b of the auto-solvolysis reaction. In addition, the rate-determining step of aluminum deposition has been reported to be either a chemical step, releasing the complexing agent chloride while aluminum is in the divalent oxidation state ($AlCl_3^- \rightarrow AlCl_2 + Cl^-$) or a double occurrence of an electron transfer from the divalent to the monovalent aluminum ($Al^{2+} + e^- \rightarrow Al^+$), based on cathodic Tafel slope evaluation from current step experiments [11]. From the above discussions, it is important to consider the intermediate reactions in developing a continuum physics-based model as they provide insights into understanding the underlying electrochemical processes. However, to the best of our knowledge, there have been no reports on developing a continuum physics-based model for RABs with (EMIMCl)-$AlCl_3$ IL electrolyte that considers all the intermediate reactions based on experiments and ab initio simulations.

In this study, we developed a high-fidelity physics-based model, which considers the successive electron transfer reactions as well as the (de)chlorination reactions at the Al metal/IL electrolyte interface to explain the plating-stripping mechanisms at different current densities in rechargeable aluminum batteries with (EMIMCl)-$AlCl_3$ IL electrolyte. The plating and stripping mechanisms considered in this model were obtained from density functional theory (DFT) calculations. The developed model is validated by comparing the model predictions with experimentally measured potential profiles at different current densities and cycling conditions obtained from Swagelok symmetrical cells composed of Al metal working and counter electrode and (EMIMCl)-$AlCl_3$ IL electrolyte. To identify the most sensitive parameters in the physics-based model, we adopted a Gaussian process regression model to perform a sensitivity analysis of the various input parameters on the cell potential and concentration during plating and stripping.

2. Model development

The model designed in this study is for predicting the galvanostatic plating and stripping of Al in a symmetrical cell composed of Al working, counter, and reference electrode with an EMIMCl-$AlCl_3$ IL electrolyte (molar ratio of 1:1.5) assembled in a Swagelok tee fitting. A schematic representation of the interfacial region of the Al working electrode, the diffusion layer, and the reaction steps that are significant to the model equations during the plating and stripping process is shown in Fig. 1a and 1b, respectively. The diffusion layer for the electroactive species, $AlCl_4^-$ and $Al_2Cl_7^-$ extends from the Al/IL electrolyte interface to the bulk electrolyte. It is assumed that the intermediate species, $AlCl_3^-$, $AlCl_2^-$ and $AlCl^-$, and Cl^- generated at the Al/IL electrolyte interface do not diffuse into the bulk electrolyte.

The three main rate-determining steps considered in modeling the plating-stripping mechanisms are (i) charge transfer to and from the intermediate species, $AlCl_3^-$, $AlCl_2^-$ and $AlCl^-$ during plating and stripping, respectively (ii) transport of the electroactive species, $Al_2Cl_7^-$ and $AlCl_4^-$, in the diffusion layer, and (iii) (de)chlorination reaction at the Al/IL electrolyte interface. The corresponding reactions are presented in Fig. 1.

During the plating of Al, the Lewis acidic heptachloroaluminate anion, $Al_2Cl_7^-$ in the bulk electrolyte is transported to the Al/IL electrolyte interface where it is reduced in a single electron transfer reaction to adsorbed $*AlCl_3^-$ and $AlCl_4^-$ species (reaction (2)). The $AlCl_4^-$ species is transported into the bulk electrolyte while the adsorbed $*AlCl_3^-$ species is further reduced in two subsequent single electron transfer

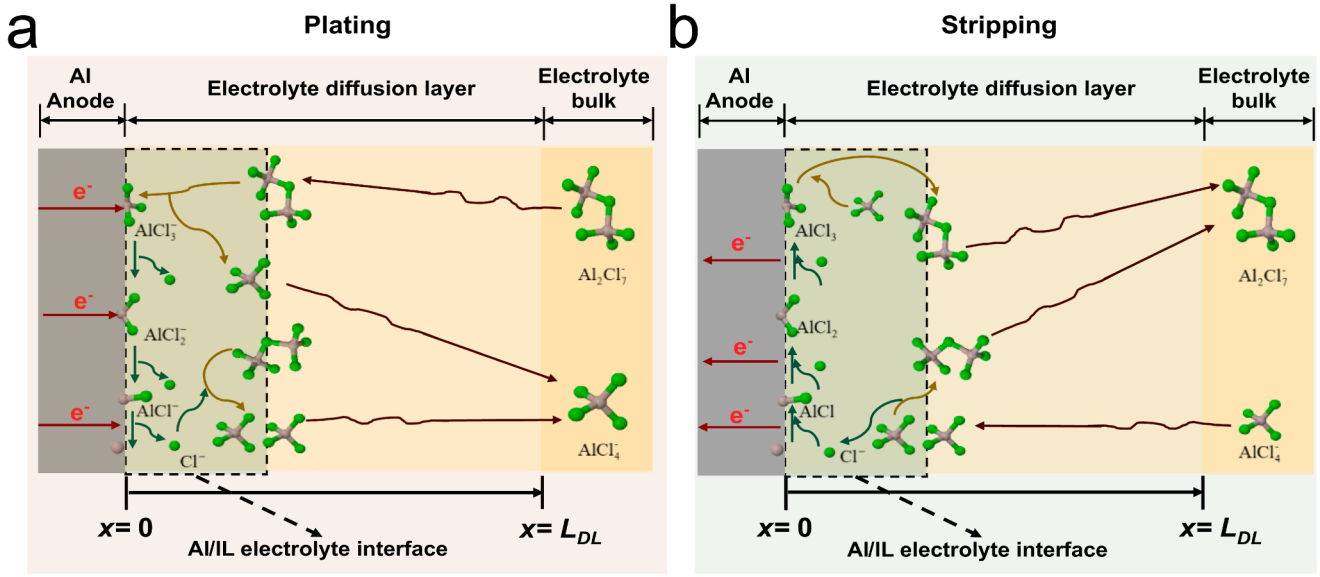

Fig. 1. Proposed plating-stripping mechanism of Al in EMIMCl-$AlCl_3$ IL electrolyte considered in this study. a, b Schematic diagram of the interfacial region closer to the Al metal working electrode surface, electrolyte diffusion layer, bulk electrolyte, and the relevant reactions during (a) plating and (b) stripping.

reduction-dechlorination reactions to $*AlCl_2^-$ and to $*AlCl^-$ (reactions (3) and (4)). The $*AlCl^-$ species undergoes a dechlorination reaction to produce *Al as shown in reaction (5). The Cl^- ions produced in reactions (2), (3) and (4) , react with $Al_2Cl_7^-$ in an equilibrium reaction (6) at the Al/IL electrolyte interface to form $AlCl_4^-$ which are transported into the bulk electrolyte. The reactions for the plating mechanism are thermodynamically verified by DFT calculations and are given as

$$Al_2Cl_7^- + e^- \overset{k_{plat,1}}{\rightarrow} *AlCl_3^- + AlCl_4^- \quad (2)$$

$$*AlCl_3^- + e^- \overset{k_{plat,2}}{\rightarrow} *AlCl_2^- + Cl^- \quad (3)$$

$$*AlCl_2^- + e^- \overset{k_{plat,3}}{\rightarrow} *AlCl^- + Cl^- \quad (4)$$

$$*AlCl^- \overset{k_{dech}}{\rightarrow} *Al + Cl^- \quad (5)$$

$$Al_2Cl_7^- + Cl^- \underset{k_{b,1}}{\overset{k_{f,1}}{\longleftrightarrow}} 2AlCl_4^- \quad (6)$$

where $k_{plat,1}$, $k_{plat,2}$ and $k_{plat,3}$ represent the rate constant for the electrochemical reduction-dechlorination reactions, and $k_{f,1}$ and $k_{b,1}$ represent the rate constant for the equilibrium reaction occurring at the Al/IL interface. The equilibrium reaction (6), is the EMIMCl-$AlCl_3$ solvent equivalent reaction of the autoionization of water but with $Al_2Cl_7^-$ and Cl^- as the Lewis acidic and basic species, respectively [30], as used in previous models [17,31]. The equilibrium constant for the reaction is given as

$$K_{eq} = \frac{\left(c_{AlCl_4^-}\right)^2}{\left(c_{Al_2Cl_7^-}\right)\left(c_{Cl^-}\right)} = \frac{k_{f,1}}{k_{b,1}} \quad (7)$$

During the stripping of Al, the tetrachloroaluminate anion electroactive species, $AlCl_4^-$ in the bulk electrolyte is transported to the Al/IL electrolyte interface, where it dissociates to form $Al_2Cl_7^-$ and Cl^- ions in equilibrium reaction (6). The $Al_2Cl_7^-$ ion is transported to the bulk electrolyte while the Cl^- ion undergoes a single electron transfer oxidation-chlorination reaction to form adsorbed $*AlCl$(reaction (7)). The $*AlCl$ undergoes two subsequent oxidation-chlorination reactions to form $*AlCl_2$ and $*AlCl_3$ in reactions (8) and (9), respectively. The $*AlCl_3$ species reacts with the tetrachloroaluminate anions ($AlCl_4^-$) at the Al/IL electrolyte interface to form the heptachloroaluminate anions ($Al_2Cl_7^-$) as shown in reaction (10), which are transported into the bulk electrolyte. Similar to the reaction steps for plating, the reaction route for stripping has been thermodynamically confirmed via DFT calculation and are given as

$$*Al + Cl^- \overset{k_{strip,1}}{\rightarrow} *AlCl + e^- \quad (8)$$

$$*AlCl + Cl^- \overset{k_{strip,2}}{\rightarrow} *AlCl_2 + e^- \quad (9)$$

$$*AlCl_2 + Cl^- \overset{k_{strip,3}}{\rightarrow} *AlCl_3 + e^- \quad (10)$$

$$*AlCl_3 + AlCl_4^- \overset{k_{f,2}}{\rightarrow} Al_2Cl_7^- \quad (11)$$

where $k_{strip,1}$, $k_{strip,2}$ and $k_{strip,3}$ represent the rate constant for the electrochemical oxidation-chlorination reactions, and $k_{f,2}$ represents the rate constant for reaction (11) at the Al/IL electrolyte interface. In reactions (2)–(4) and reactions (8)–(10), the elementary steps are described as concerted chloride-electron transfer reactions to reduce the complexity in the physics-based model development.

In summary, the physics-based model was developed based on the dilute solution theory, and the model equations are related to material balance on the electroactive and intermediate species in the IL electrolyte. Ohm's law was used to describe the transfer of charges in the solid and liquid phases. The Butler-Volmer equation was used to describe the rate of the electrochemical-(de)-chlorination reaction at the electrode/IL electrolyte interface. The Butler-Volmer equation was modified such that the rate constants were based on the transition-state theory and allowed the inclusion of the activation energy for each of the electrochemical reactions. Finally, we derived a mathematical expression to describe the electrolyte concentration overpotential by integrating the solution phase current density. A detailed description of the physics-based model governing equations and parameters is presented in the Supplementary Material.

3. Experiments

3.1. Materials and electrode preparation

Al disc working and counter electrodes used in the Swagelok cells had a diameter of 6 mm (99.999 % purity, Advent Research Materials) embedded in a 10.4 mm diameter PTFE shroud. The disc electrodes were polished to a mirror finish with SiC grinding paper (Struers, mesh size #1200, #2400, and #4000) followed by polishing with 3 μm diamond suspension (Struers), cleaned with soap and rinsed with distilled water. The Al electrodes were then sonicated in an ultrasonic bath (Emag Germany emmi-4®) with ethanol (ROTH ethanol 96%) for half a minute, followed by a rinse with deionized water and drying in an oven for 48 h at 60 °C before transferring them into the glovebox. The quasi-reference electrode was an Al wire with 1 mm diameter (99.999% purity, Advent Research Materials). The ionic liquid 1.5:1 mixture of $AlCl_3$ and 1-ethyl-3-methylimidazolium chloride (≥95%) was purchased from Sigma-Aldrich.

3.2. Electrochemical characterization

Battery cells made from PFA Swagelok tee fittings (1/2 in. diameter) were used in three-electrode configuration for galvanostatic cycling experiments. The Swagelok cells equipped with working and counter electrodes were filled in the glovebox with the IL electrolyte through the opening for the reference electrode, fitted with the reference electrode, closed tightly, and connected to a Basytec CTS LAB XL (Basytec GmbH, Asselfingen, Germany) for galvanostatic cycling outside the glovebox. The open circuit potential of each cell was monitored during soaking for 54 h, before 10 cycles at each current density i of 0.217, 0.726, 1.000, and 1.453 mA cm^{-2} and a charge density of 1 mAh cm^{-2} per half-cycle were measured. The initial half-cycle of the working electrode was charging, and after each half-cycle the cell rested at OCP for 1 min. In the continuous system, three different cells were cycled continuously at different current densities (Fig. S1), while in the batch system four different cells were cycled each at a different current density (Fig. S2).

3.3. Density function theory calculations

We model the reactions with density functional theory (DFT). Calculations were performed with the BEEF-vdW exchange–correlation functional [32] using the GPAW code [33] version 21.6.0. We employ a continuum solvent model (CSM) [34] to take into account the adsorbate's interaction with the ionic liquid molecules.

The CSM model implemented in GPAW has a few parameters that need to be determined for the IL (EMIMCl)-$AlCl_3$. Firstly, the static dielectric constant we use a value of 15 [16]. Secondly, the CSM model maintains a cavity around a solute (in this case an adsorbate), this cavity is created with a repulsive potential with one free parameter (u0), which is the value of the potential at the van der Waals radius. We determine u0 to 175 meV, using a procedure equal to the one described in detail for BMIM in [34]. The procedure entails, in short: Relax positive ($EMIM^+$) and negative ($AlCl_4^-$) parts of the IL, calculating cavity volume using the GPAW implementation, comparing the sum of the two volumes with the molar volume of the EMIMCl-$AlCl_3$ 1:1.5 mixture, given the density

1.304 g/mL, vary u0 until the volumes match. In this procedure, we assume that the volume of an IL can be given as the sum of the cation and anion volumes [35]. For the compressibility, we use a value of 3.3e10 Pa^{-1} found for the closely related IL [EMIM][BF4] [35], which has an almost negligible effect on the determination of u0. The last parameter is the surface tension of the cavity; however, since we are only interested in energy differences of very similar structures with similar cavity surface areas, the effect of the surface tension parameter is negligible. A few tests confirming this statement is available at [36].

To ensure that we obtain energies of the adsorbate species from their most favorable configurations, we employ a form of constrained minima hopping [37], where the molecular identity of the adsorbate is maintained during the algorithm that entails molecular dynamics and local relaxation. Energy barriers between molecular states (e.g., *AlCl + *Cl -> $*AlCl_2$) were determined using the climbing image Nudged Elastic Band (NEB) [38] method. The constrained minima hopping and NEB algorithms are implemented in the Atomic Simulation Environment (ASE) [39], which was also used to setup and analyze the results of the calculations.

An aluminum surface was modeled using a 4-layer Al fcc slab (lattice constant 4.05 Å) exposing the (1 1 1) surface. To ensure negligible interaction between the adsorbate periodic images, the unit cell contained 5x5 atoms in each direction in the surface as well as 20 Å of vacuum between slabs. Thus, the computational slab totals 100 atoms. The unit cells are fixed during atomic relaxation, and so are the bottom two layers of the slab to emulate the interaction with a bulk region.

4. Results and discussion

4.1. Density functional theory calculations

The Al stripping was modeled through free Cl and Al on the Al(1 1 1) surface. First, the most stable adsorption sites of all species were determined; Al adsorbs on the slab (denoted by *Al) in a 3-fold coordinated hcp site, *Cl adsorbs on an on top site. As Cl connects to the undercoordinated Al on the slab, the most favorable adsorbate position switches to less coordinated sites, i.e., *AlCl prefers hcp site, $*AlCl_2$ sits in bridge site whereas $*AlCl_3$ takes up an on top site (see also the inset atomic illustrations in Fig. 2). The first two chlorination steps have small energy barriers associated with the rearrangement of the adsorbate species; the final barrier is more significant, i.e., *Al + *Cl -> *AlCl (Fig. 2a and 2b) and *AlCl + *Cl -> $*AlCl_2$ (Fig. 2a and 2c) has a barrier of 5.5 and 1.9 kJ/mol respectively and $*AlCl_2$ + *Cl -> $*AlCl_3$ (Fig. 2a and 2d) has a barrier of 16 kJ/mol as determined with NEB calculations. This, however, only accounts for the barrier when the two adsorbed species sit right next to each other on the slab, a migration of one (or both) of the species has to take place for that to happen. The *Cl migration between on top sites (see inset in Fig. 2a) has an associated 29

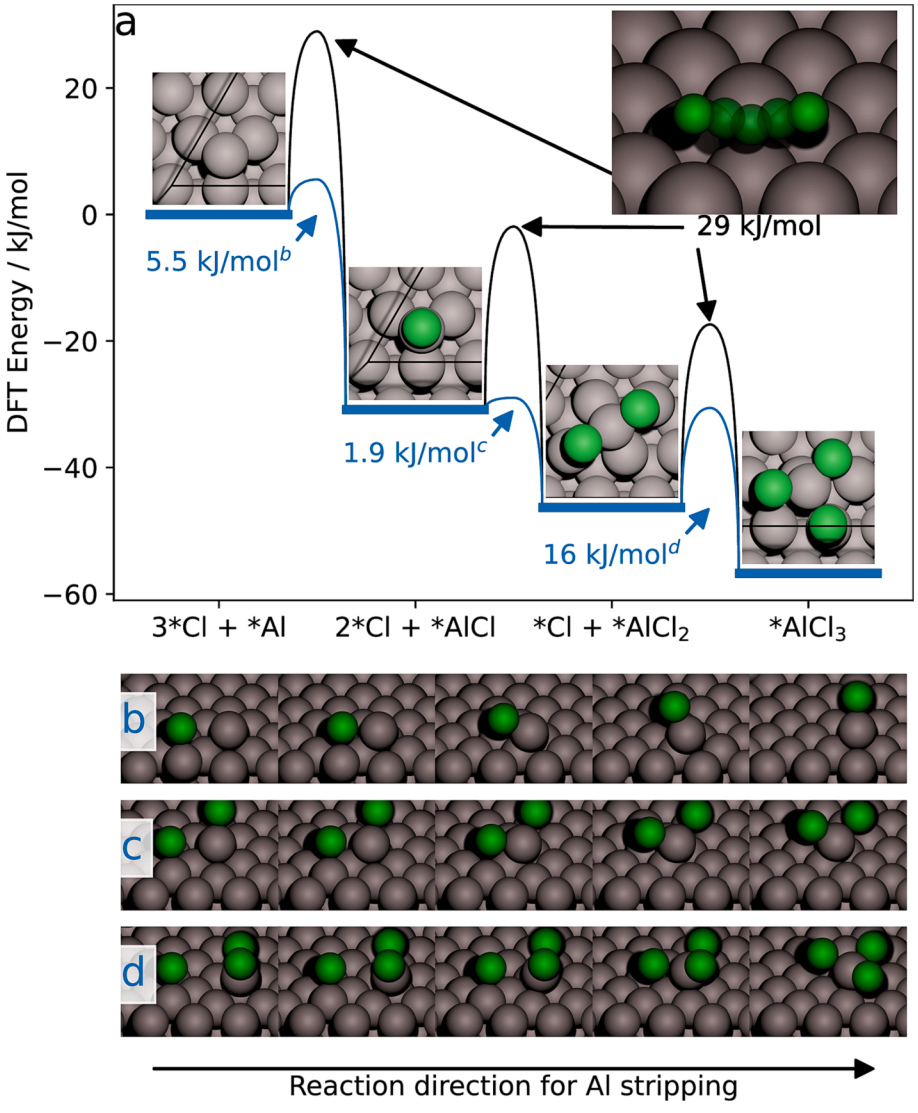

Fig. 2. (a) DFT calculation of energy barriers for (de) chlorination reaction at the (1 1 1) surface of Al metal. The thick horizontal lines are the energy levels at each reaction step as described in the text. The insets above each energy level show the atomic structure with the adsorbate species at the most stable site. The blue lines between energy levels show the energy barrier for the corresponding reaction; the barriers' heights are noted below the energy levels. The black lines between energy levels show the energy barrier of a Cl atom moving between two sites on the surface; this is also depicted in the inset in the top right corner. The atoms coloring is for all images: Grey: Al, green: Cl. (b) The NEB path in 5 images of the *Al + *Cl -> *AlCl reaction. The leftmost and rightmost images are the initial and final configurations, respectively. The middle image is the transition state giving rise to the barrier. (c) NEB path of the *AlCl + *Cl -> $*AlCl_2$ reaction. d: NEB path of the $*AlCl_2$ + *Cl -> $*AlCl_3$ reaction. (For interpretation of the references to colour in this figure legend, the reader is referred to the web version of this article.)

kJ/mol barrier; thus, this is used as the effective barrier for each step in the energy diagram, Fig. 2. The first chlorination step forming *AlCl is the most favorable reaction, gaining 31 kJ/mol. The final two steps gain 15 kJ/mol and 13 kJ/mol, respectively. The energy gains can be read off the graph as the energy distance between the thick horizontal blue lines.

4.2. Physics-based model validation

The fidelity of the physics-based model was validated by comparing the model predictions at current densities of 0.22, 0.73, 1.0, and 1.45 mA cm^{-2} to experimental data obtained from a Swagelok cell composed of an EMIMCl-$AlCl_3$ IL electrolyte and Al working, counter, and reference electrode. We first fitted the model predictions to the potential profile at the continuous system's low current density of 0.22 mA cm-2, where the rate performance was conducted on a single cell (Fig. S1). Three cells were used for this experiment to ensure precision, but there was no significant difference between the cell potential at a given current density and cycle number; hence we selected the third cycle at each current density during plating and stripping for the model validation and present the results in Fig. 3a and 3b, respectively. The model predictions were made with the nominal parameters in Table S1. The validated model was then used to predict and fit the experimental data at higher current densities and the batch system, where each cell was cycled at a different current rate (Fig. 3c and 3d) while treating the diffusion coefficients, area factor, and the standard equilibrium potential as fitting parameters. There was good agreement between the model predictions and the experimental data suggesting that the developed model can replicate the plating-stripping mechanism of RABs with imidazolium-based IL electrolytes.

4.3. Parametric analysis of physics-based model

To have an extensive insight into the plating-stripping mechanisms concerning the relevant limitations, we conducted a detailed analysis of the variation in the fitting parameters and presented them in Fig. 4. The values of these parameters were obtained by fitting the model-predicted working electrode potential at the various current densities and cycling conditions to those of the experimental data using a Nelder-Mead least-square technique. This method of identifying input parameters in electrochemical models has been adopted in previous studies and has proven reliable and effective [40–42]. During plating, the diffusion coefficient of $AlCl_4^-$, $Al_2Cl_7^-$ and $EMIM^+$ increased exponentially as the current density was increased from 0.22 mA cm^{-2} to 0.73 mA cm^{-2} and remained fairly constant at the higher current densities of 1 mA cm^{-2} and 1.45 mA cm^{-2} for both the continuous and the batch system. For stripping, the diffusion coefficient remained constant at all current densities for $EMIM^+$ and $Al_2Cl_7^-$ species but decreased with increasing current density for $AlCl_4^-$. The area factor is a correction factor that accounts for variations in the locations of the dividing surfaces that defines a successful reaction. It varied with the current density for both batch and continuous systems during plating and striping. Still, the

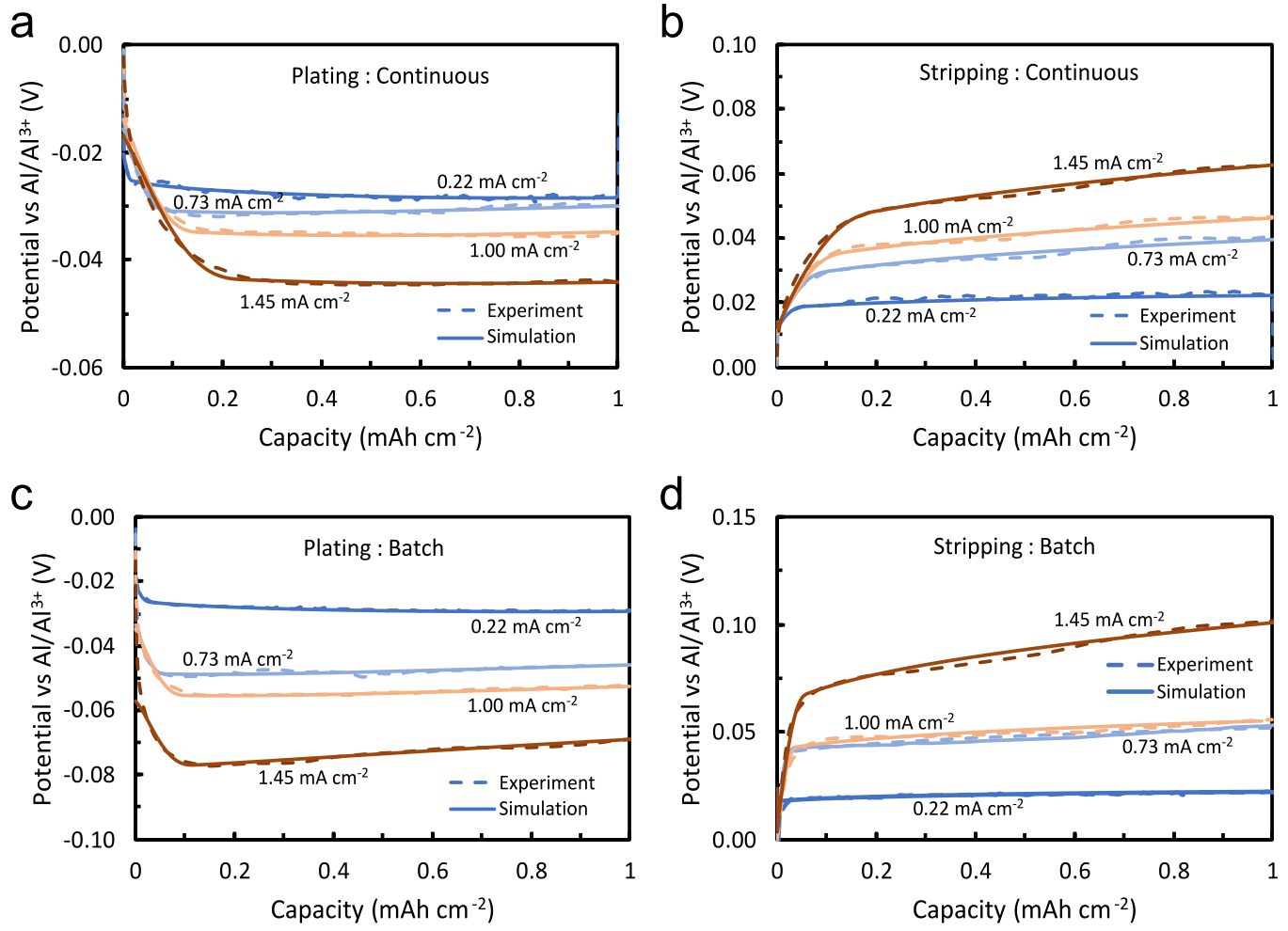

Fig. 3. Physics-based model validation with experimental data. Model best fit to experimental data: Working electrode potential in a single Al-Al symmetrical cell continuously cycled at different current densities (continuous system) during (a) plating and (b) stripping. c, d Working electrode potential in different Al-Al symmetrical cells cycled at a given current density (batch system) during (c) plating and (d) stripping.

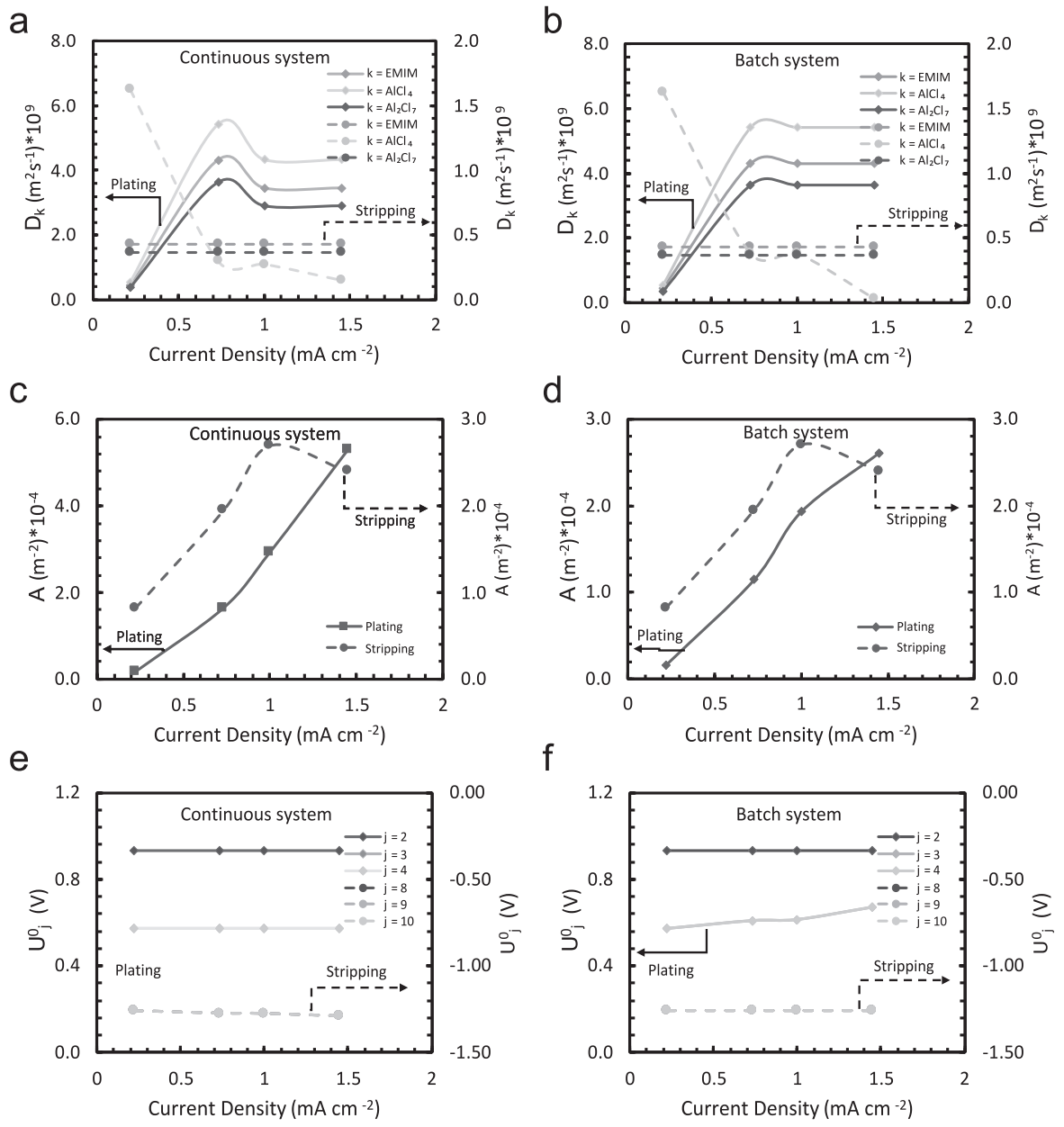

Fig. 4. Parametric insight into the plating-stripping mechanism of Al in (EMIMCl)-$AlCl_3$ IL electrolyte as a function of current density. a, b Variations in diffusion coefficient (D_k) for (a) continuous and (b) batch systems. c, d Changes in area factor (A) for (c) continuous and (d) batch systems. e, f Variations in standard equilibrium potential (U_j^0) (e) continuous and (f) batch systems. The values of the fitting parameters were evaluated by fitting the model predictions to the experimental potential profiles using the Nelder-Mead least-square fitting technique.

standard equilibrium potential for a given electrochemical reaction showed only little or no significant changes with variation in the current density. The major difference in the continuous and batch system is the rate at which the area factor increased with increasing current density during plating, which was two times higher for the former than the latter. This indicates that the electrochemical reaction rate at the Al/IL electrolyte interface was faster for the continuous system than the batch system due to the more extensive removal of the oxide film on the Al metal anode at higher concentrations of $Al_2Cl_7^-$ species with prolonged cycling [10]. The area factor increased with increasing current density but decreased at a current density of 1.45 mA cm^{-2} during striping for both the continuous and batch system in Fig. 4c and 4d, respectively. The decrease in the area factor at high current density during stripping is attributed to the low concentration of the reacting species, $AlCl_4^-$ at the electrode/IL electrolyte interface. (Fig. S4b and S5b) Variations in the transport kinetic parameters (diffusion coefficients and area factor) in Fig. 4 suggest that the rate performance of RABs with imidazolium-based IL electrolytes is limited mainly by kinetics and slightly by diffusion.

4.4. Physics-based model predictions

Using Eq. S 17, we simulated the concentration overpotential for the electroactive species in the IL electrolyte for both the continuous and batch system and presented the results in Fig. 5 and Fig. S3, respectively. The changes in concentration of $AlCl_4^-$ species with capacity decreased with an increase in the current density from 0.73 mA cm^{-2} to 1.45 mA cm^{-2} at the working electrode, while those of $Al_2Cl_7^-$ species increased with increasing current density during plating (Fig. S4a and S4c). This resulted in an increase in the magnitude of the electrolyte concentration

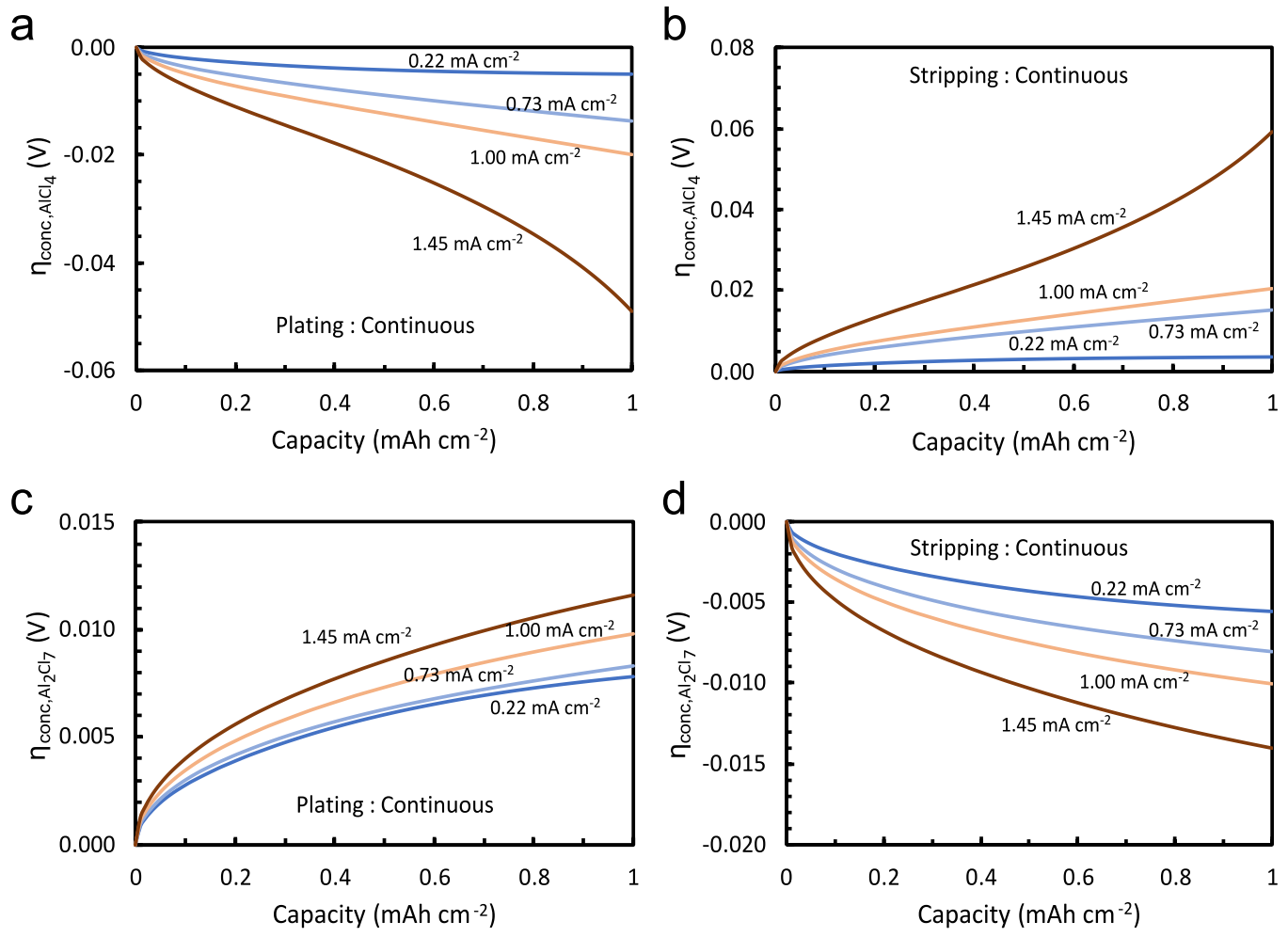

Fig. 5. Effects of current density on concentration overpotential in (EMIMCl)-$AlCl_3$ IL electrolyte. a, b Concentration overpotential for $AlCl_4^-$ species, ($\eta_{conc,AlCl_4^-}$) during (a) plating and (b) stripping. c, d Concentration overpotential for $Al_2Cl_7^-$ species, ($\eta_{conc,Al_2Cl_7^-}$) during (c) plating and (d) stripping.

overpotential with an increase in the current density from 0.22 mA cm^{-2} to 1.45 mA cm^{-2} for both species (Fig. 5a and 5c). As expected, the concentration of the $AlCl_4^-$ species reduced while that of $Al_2Cl_7^-$ species increased during stripping, with the rate being faster at higher current densities (Fig. S4b and S4d). Consequently, the magnitude of the electrolyte concentration overpotentials increased with the current density for both species during stripping (Fig. 5b and 5d). A similar trend was observed for the batch system, with the magnitude of the electrolyte concentration overpotentials (Fig. S3) being higher than those of the continuous system due to higher concentration gradients (Fig. S5). According to Eq. S17, $\eta_{conc,k}$ depends on the concentration, c_k, temperature, T, and the thickness of the diffusion layer, L_{DL}. However, the variations in $\eta_{conc,k}$ depend only on the c_k as the other parameters are constant. Thus, the increase in the magnitude of $\eta_{conc,k}$ as a function of the current densities is because of increasing concentration gradients in c_k at higher current densities.

To understand the effect of the current densities and the cycling conditions on the dynamics of the plating and stripping mechanism, we simulated the transformation of the relative concentration of deposited and stripped Al as a function of the square root of time, sqrt(t) and presented the results in Fig. 6. Define as the rate of change of the square root of time with concentration ($dt^{1/2}/dc_{Al}$), peaks in the $dt^{1/2}/dc_{Al}$ vs. $t^{1/2}$ curves caused by plateaus in the concentration profile corresponds to changes in the collective particle growth dynamics similar to the description given by Altimari et al. [43]. During the initial stages of plating (up to 16 s) $AlCl_3^-$ (Fig. S6a and 6b) is the intermediate anion that is predominantly produced through reaction (2) at the surface of the Al metal working electrode. As the plating process proceeds further, the cell potential decreases, and the reactions (3) and (4), whose standard equilibrium potentials are significantly lower, become predominant, generating $AlCl_2^-$ (Fig. S6c and 6d) and $AlCl^-$ (Fig. S6e and 6f). The intermediate anions, $AlCl^-$, undergo a kinetically controlled dechlorination reaction to deposit Al on the surface of the Al metal. Owing to the time interval required for the cell potential to decrease for all the plating reactions to occur, there were no significant changes in the relative concentration of the deposited Al during the initial stages of plating for both continuous and batch systems, as observed in Fig. S7a and S7b respectively. The time at which the deposition of Al or nucleation started decreased with an increase in the current density and was lower for the batch system than the continuous system.

After nucleation in Fig. 6a and 6b, there was a sharp increase in the $dt^{1/2}/dc_{Al}$ curve with the square root of time until it peaked at a time of ca. 440 s and 360 s for the continuous and batch system, respectively. This demonstrates the independent growth of Al particles at the beginning of the electrodeposition during plating through a diffusion-controlled process. As electrodeposition proceeds, there is an accumulation of the intermediate species at the Al metal/IL electrolyte interface, which increased the electrolyte concentration overpotential (Fig. S8), accelerating the diffusion of the electroactive species and rate of the electrochemical reactions (2), (3) and (4). However, the electrodeposition is controlled by the dechlorination reaction (5), which is only dependent on diffusion in the early stages of the electrodeposition as the

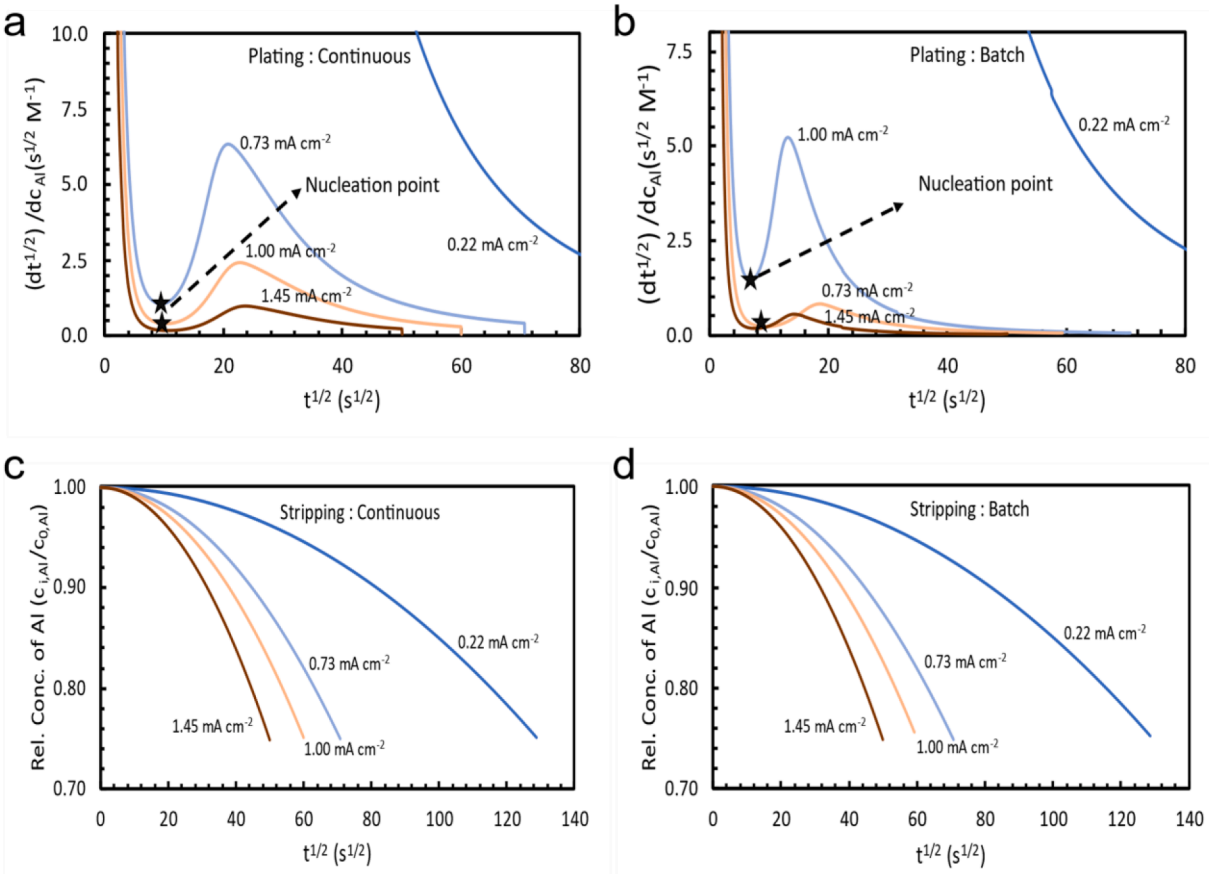

Fig. 6. Transformations of concentration of deposited and stripped Al as a function of the square root of time at different current densities. a, b Simulated $dt^{1/2}/dc_{Al}$ during plating for (a) continuous and (b) batch system. c, d Simulated relative concentration of Al during stripping for (c) continuous and (d) batch systems.

electroactive species needs to be transported to the Al metal/IL electrolyte interface for all the intermediate species to be produced. This leads to an increase in the deposition rate of Al, and the $dt^{1/2}/dc_{Al}$ curve drops to zero with a faster drop rate at higher current densities, indicating a kinetically controlled process [43]. Thus, most of the electrodeposition is controlled by kinetics as confirmed by the cyclic voltammogram results in Fig. S11 (supplementary material).

The stripping mechanism is governed by the electrochemical and chemical reactions (8), (9), (10), and (11). Unlike the plating mechanism, the stripping of Al begins at the first electrochemical reaction thus, the relative concentration of Al at the surface of the working electrode decreased instantly as the time increased and at a faster rate at higher current densities. The rate at which the relative concentration decreased at a given current density was similar for both the continuous (Fig. 6c) and the batch (Fig. 6d) systems. Thus, the limiting step for the stripping mechanism is the first electrochemical oxidation-chlorination reaction (8). The rate-determining step for the stripping mechanism, as confirmed by DFT calculations, is similar to that reported by Böttcher et al. [11].

4.5. Sensitivity analysis

To accurately match our model predictions to the experimental data, some of the model input parameters were expressed as a function of the current density using a non-linear least square regression technique, as presented in Fig. 4. These parameters were arbitrarily selected based on prior knowledge of the plating/stripping mechanism of similar electrochemical systems [44–46]. However, the choice of whether the model parameters should be a function of the current density is a tradeoff between the model's accuracy and efficiency. Such a dilemma, which is implicitly based on the assumption that all the input parameters are equally relevant to a given model output, is likely superfluous as different outputs may be more sensitive to variations of some parameters than others. This issue can be addressed by quantifying the relative importance of the input parameters via a sensitivity analysis [47,48]. Input parameters which require much effort to estimate owing to the relevance of the impact of their uncertainties on the output parameters, are also revealed through sensitivity analysis. In this regard, we conducted a global and local sensitivity analysis of all the input parameters (Table S1) using a differentiable surrogate Gaussian process (GP) regression model [48] on the two output parameters, and a detailed description of the sensitivity analysis method is described in the supplementary materials. Fig. 7a and 7b show the outcome of the sensitivity analysis of the physics-based model input parameters on the electrode potential and concentration of deposited Al, respectively.

One of the goals of this section is to quantify and compare the sensitivity of each input parameter on electrode potential at a capacity of 1 mA cm^{-2} during plating using Eq. SA-2 and the surrogate GP regression model on the validation data set in Fig. S9. The global sensitivity of all 17 input parameters for the log of the cell potential is shown in Fig. 7a. Out of the 17 parameters, the four parameters with global sensitivity of more than 0.05 are defined as sensitive parameters for the cell potential. All the four sensitive parameters, pre-exponential factor, activation barrier for plating, and standard equilibrium potential for reactions (2) and (3), are related to the kinetic properties. Surprisingly, the parameters related to transport properties in the electrolyte (diffusion coefficients of the electroactive species) were not sensitive to the cell potential at a capacity of 1 mA cm^{-2}. This is because, according to Fig. 4a and 4b, the diffusion coefficient only changes at low current densities where there is no significant difference between the electrode

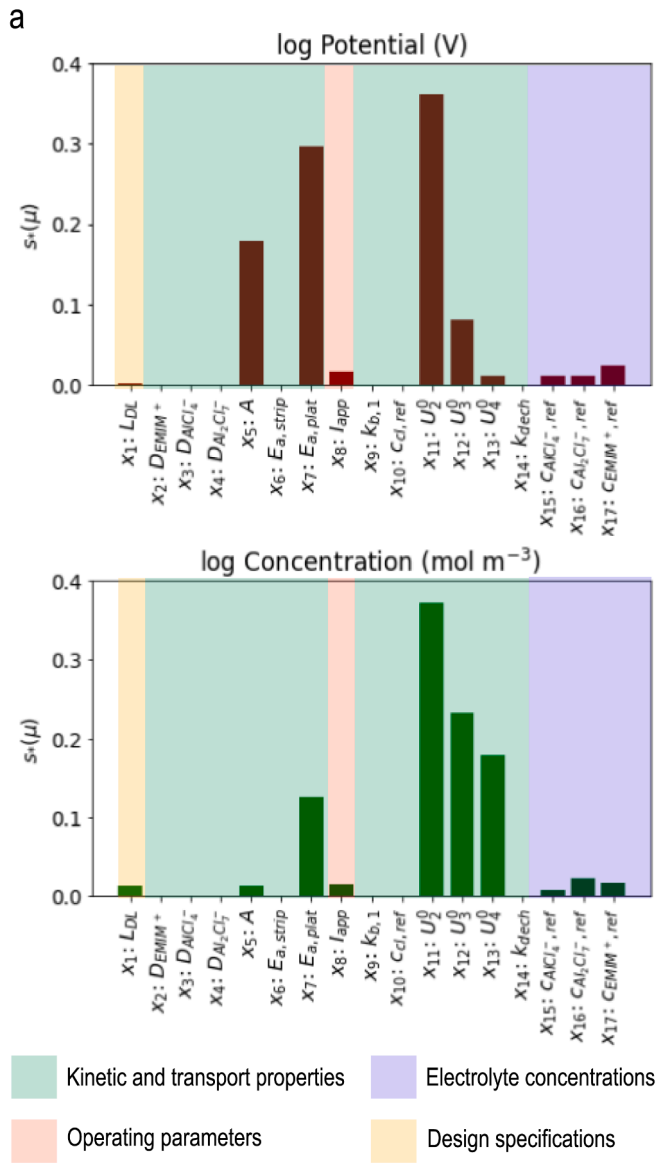

Fig. 7. Sensitivity analysis of physics-based model parameters. a, b Normalized global parameter sensitivity for (a) Electrode potential and (b) concentration of deposited Al at the end of plating.

potential at the end of the plating process at 0.22 mA cm^{-2} and 0.73 mA cm^{-2} (Fig. 3a). We also conducted a global sensitivity analysis of the 17 input parameters on the log of the deposited Al concentration at the Al metal's surface. We presented the results in Fig. 7b. Four input parameters, the activation barrier for plating and the standard equilibrium potential for reactions (2), (3), and (4), were identified as the most sensitive parameters. In addition, the diffusion layer thickness also exhibited a significant sensitivity, indicating that the diffusion length of the electroactive species (transport properties) plays an important role in the plating mechanism. The results in Fig. 7 demonstrate that much effort should be made in estimating the relevant input parameters, such as the activation barriers and the standard equilibrium potential for the electrochemical reactions. In contrast, the other parameters can be estimated roughly since their uncertainties have no significant impact on the output results.

5. Conclusion

We have elucidated the plating-stripping mechanism of aluminum ion batteries with (EMIMCl)-$AlCl_3$ IL electrolyte via an experimentally validated physics-based model augmented with DFT calculations and machine learning models at different current densities and cycling conditions. Based on our estimated barrier for creating the species involved in the proposed reactions for Al stripping and plating with DFT calculations, we found out that the largest barrier comes from the migration of single Cl atoms on the Al surface. This migration needs to take place even if the actual reaction mechanism for Al stripping/plating is different, thus, the 29 kJ/mol barrier will always be a lower bound on the actual barrier. Evidenced by extensive parametric analysis, we found a faster electrochemical reaction at the Al/IL electrolyte interface for the continuous system, in which the native oxide on the surface of the Al electrode is assumed to be completely removed, and the performance of the cells was kinetically limited at high current densities. Owing to the accumulation of intermediate and electroactive species at the surface of the Al metal due to transport limitations, high electrolyte concentration and ohmic overpotentials were observed at low current densities during the plating of Al. Our analysis of the concentration of the deposited Al revealed that the electrodeposition mechanism is governed mainly by kinetics with diffusion-control at the early stages, and the most sensitive parameters to this mechanism are the activation barrier and the standard equilibrium potential for the (de) chlorination-electrochemical reactions (2) and (10) for plating and stripping respectively. The developed physics-based model can be applied to design and optimize other (EMIMCl)-$AlCl_3$ IL electrolyte-based aluminum battery systems with slight modification at the cathode. This work highlights the assurance of combining models at different scales, machine learning algorithms, and experiments for understanding and developing sophisticated electrochemical systems such as rechargeable aluminum batteries with imidazolium-based IL electrolytes.

Declaration of Competing Interest

The authors declare that they have no known competing financial interests or personal relationships that could have appeared to influence the work reported in this paper.

Data availability

Data will be made available on request.

Appendix A. Supplementary data

Supplementary data to this article can be found online at https://doi.org/10.1016/j.cej.2023.144995.

References

[1] G.A. Elia, K. Marquardt, K. Hoeppner, S. Fantini, R. Lin, E. Knipping, W. Peters, J.-F. Drillet, S. Passerini, R. Hahn, G.A. Elia, K. Marquardt, K. Hoeppner, S. Fantini, R. Lin, W. Peters, J.F. Drillet, S. Passerini, R. Hahn, An overview and future perspectives of aluminum batteries, Adv. Mater. 28 (2016) 7564–7579, https://doi.org/10.1002/ADMA.201601357.

[2] V. Verma, S. Kumar, W. Manalastas, R. Satish, M. Srinivasan, Progress in rechargeable aqueous zinc- and aluminum-ion battery electrodes: challenges and outlook, Adv. Sustain. Syst. 3 (1) (2019), 1800111, https://doi.org/10.1002/ADSU.201800111.

[3] M.C. Lin, M. Gong, B. Lu, Y. Wu, D.Y. Wang, M. Guan, M. Angell, C. Chen, J. Yang, B.J. Hwang, H. Dai, An ultrafast rechargeable aluminium-ion battery, Nature 520 (2015) 325–328, https://doi.org/10.1038/nature14340.

[4] K.V. Kravchyk, S. Wang, L. Piveteau, M.V. Kovalenko, Efficient aluminum chloride-natural graphite battery, Chem. Mater. 29 (2017) 4484–4492, https://doi.org/10.1021/ACS.CHEMMATER.7B01060/ASSET/IMAGES/LARGE/CM-2017-01060M_0005.JPEG.

[5] O.M. Leung, T. Schoetz, T. Prodromakis, C. Ponce de Leon, Review—progress in electrolytes for rechargeable aluminium batteries, J. Electrochem. Soc. 168 (5) (2021), 056509, https://doi.org/10.1149/1945-7111/ABFB36.

[6] H. Chen, H. Xu, B. Zheng, S. Wang, T. Huang, F. Guo, W. Gao, C. Gao, Oxide film efficiently suppresses dendrite growth in aluminum-ion battery, ACS Appl. Mater. Interfaces. 9 (2017) 22628–22634, https://doi.org/10.1021/ACSAMI.7B07024/SUPPL_FILE/AM7B07024_SI_003.MPG.

[7] F. Wu, N. Zhu, Y. Bai, Y. Gao, C. Wu, An interface-reconstruction effect for rechargeable aluminum battery in ionic liquid electrolyte to enhance cycling performances, Green Energy Environ. 3 (2018) 71–77, https://doi.org/10.1016/J.GEE.2017.10.002.

[8] S. Choi, H. Go, G. Lee, Y. Tak, Electrochemical properties of an aluminum anode in an ionic liquid electrolyte for rechargeable aluminum-ion batteries, Phys. Chem. Chem. Phys. 19 (2017) 8653–8656, https://doi.org/10.1039/C6CP08776K.

[9] N.a. Zhu, K. Zhang, F. Wu, Y. Bai, C. Wu, Ionic Liquid-Based Electrolytes for Aluminum/Magnesium/Sodium-Ion Batteries, Energy Mater Adv (2021), https://doi.org/10.34133/2021/9204217.

[10] H. Wang, S. Gu, Y. Bai, S. Chen, N. Zhu, C. Wu, F. Wu, Anion-effects on electrochemical properties of ionic liquid electrolytes for rechargeable aluminum batteries, J. Mater. Chem. A. 3 (2015) 22677–22686, https://doi.org/10.1039/C5TA06187C.

[11] R. Böttcher, S. Mai, A. Ispas, A. Bund, Aluminum deposition and dissolution in [emim]cl-based ionic liquids-kinetics of charge-transfer and the rate-determining step, J. Electrochem. Soc. 167 (10) (2020), 102516, https://doi.org/10.1149/1945-7111/AB9C84.

[12] C. Wang, A. Creuziger, G. Stafford, C.L. Hussey, Anodic dissolution of aluminum in the aluminum chloride-1-ethyl-3-methylimidazolium chloride ionic liquid, J. Electrochem. Soc. 163 (2016) H1186–H1194, https://doi.org/10.1149/2.1061614JES/XML.

[13] A. Bakkar, V. Neubert, Electrodeposition and corrosion characterisation of micro- and nano-crystalline aluminium from AlCl3/1-ethyl-3-methylimidazolium chloride ionic liquid, Electrochim. Acta. 103 (2013) 211–218, https://doi.org/10.1016/J.ELECTACTA.2013.03.198.

[14] N. Jayaprakash, S.K. Das, L.A. Archer, The rechargeable aluminum-ion battery, Chem. Commun. 47 (2011) 12610–12612, https://doi.org/10.1039/C1CC15779E.

[15] S. Wang, Z. Yu, J. Tu, J. Wang, D. Tian, Y. Liu, S. Jiao, S. Wang, Z.J. Yu, J.G. Tu, J. X. Wang, D.H. Tian, S.Q. Jiao, Y.J. Liu, A novel aluminum-ion battery: Al/AlCl3-[EMIm]Cl/Ni3S2@graphene, Adv. Energy Mater. 6 (2016) 1600137, https://doi.org/10.1002/AENM.201600137.

[16] A. Bhowmik, D. Carrasco-Busturia, P. Jankowski, R. Raccichini, N. Garcia-Araez, J. M. García-Lastra, Influence of ionic coordination on the cathode reaction mechanisms of Al/S batteries, J. Phys. Chem. C. 126 (2022) 40–47, https://doi.org/10.1021/ACS.JPCC.1C08426.

[17] S. Schaltin, M. Ganapathi, K. Binnemans, J. Fransaer, Modeling of aluminium deposition from chloroaluminate ionic liquids, J. Electrochem. Soc. 158 (2011) D634, https://doi.org/10.1149/1.3623781.

[18] T. Gao, X. Li, X. Wang, J. Hu, F. Han, X. Fan, L. Suo, A.J. Pearse, S.B. Lee, G. W. Rubloff, K.J. Gaskell, M. Noked, C. Wang, A rechargeable Al/S battery with an ionic-liquid electrolyte, Angew. Chemie Int. Ed. 55 (2016) 9898–9901, https://doi.org/10.1002/anie.201603531.

[19] C. Ferrara, V. Dall'Asta, V. Berbenni, E. Quartarone, P. Mustarelli, Physicochemical characterization of AlCl 3 –1-Ethyl-3-methylimidazolium chloride ionic liquid electrolytes for aluminum rechargeable batteries, J. Phys. Chem. C 121 (48) (2017) 26607–26614.

[20] T. Jiang, M.J. Chollier Brym, G. Dubé, A. Lasia, G.M. Brisard, Electrodeposition of aluminium from ionic liquids: Part I-electrodeposition and surface morphology of aluminium from aluminium chloride (AlCl3)-1-ethyl-3-methylimidazolium chloride ([EMIm]Cl) ionic liquids, Surf. Coatings Technol. 201 (1-2) (2006) 1–9.

[21] W.A. Appiah, H. Li, J. Lampkin, J.M. García-Lastra, Towards understanding aluminum sulfur batteries with imidazolium-based electrolytes: a phenomenological model, J. Power Sources. 529 (2022), 231254, https://doi.org/10.1016/J.JPOWSOUR.2022.231254.

[22] A.J. Bard, L.R. Faulkner, Electrochemical methods : fundamentals and applications, Wiley, 2001 https://www.wiley.com/en-us/Electrochemical+Methods%3A+Fundamentals+and+Applications%2C+2nd+Edition-p-9780471043720 (accessed June 24, 2019.

[23] A. Endo, M. Miyake, T. Hirato, Electrodeposition of aluminum from 1,3-dimethyl-2-imidazolidinone/AlCl3 baths, Electrochim. Acta. 137 (2014) 470–475, https://doi.org/10.1016/J.ELECTACTA.2014.06.044.

[24] J. Wang, X. Zhang, W. Chu, S. Liu, H. Yu, A sub-100 ° C aluminum ion battery based on a ternary inorganic molten salt, Chem. Commun. 55 (2019) 2138–2141, https://doi.org/10.1039/C8CC09677E.

[25] J. Tu, J. Wang, H. Zhu, S. Jiao, The molten chlorides for aluminum-graphite rechargeable batteries, J. Alloys Compd. 821 (2020), 153285, https://doi.org/10.1016/J.JALLCOM.2019.153285.

[26] C. von Lüders, J. Keil, M. Webersberger, A. Jossen, Modeling of lithium plating and lithium stripping in lithium-ion batteries, J. Power Sources. 414 (2019) 41–47, https://doi.org/10.1016/J.JPOWSOUR.2018.12.084.

[27] T. Sun, T. Shen, Y. Zheng, D. Ren, W. Zhu, J. Li, Y. Wang, K. Kuang, X. Rui, S. Wang, L. Wang, X. Han, L. Lu, M. Ouyang, Modeling the inhomogeneous lithium plating in lithium-ion batteries induced by non-uniform temperature distribution, Electrochim. Acta. 425 (2022), 140701, https://doi.org/10.1016/J.ELECTACTA.2022.140701.

[28] S. Hein, T. Danner, A. Latz, An Electrochemical model of lithium plating and stripping in lithium ion batteries, ACS Appl. Energy Mater. 3 (2020) 8519–8531, https://doi.org/10.1021/ACSAEM.0C01155/ASSET/IMAGES/LARGE/AE0C01155_0009.JPEG.

[29] W. Mei, L. Zhang, J. Sun, Q. Wang, Experimental and numerical methods to investigate the overcharge caused lithium plating for lithium ion battery, Energy Storage Mater. 32 (2020) 91–104, https://doi.org/10.1016/J.ENSM.2020.06.021.

[30] B. Trémillon, G. Letisse, Proprietes en solution dans le tetrachloroaluminate de sodium fondu I. systemes "acide-base", J. Electroanal. Chem. Interfacial Electrochem. 17 (1968) 371–386, https://doi.org/10.1016/S0022-0728(68)80217-7.

[31] P.K. Lai, M. Skyllas-Kazacos, Electrodeposition of aluminium in aluminium chloride/1-methyl-3-ethylimidazolium chloride, J. Electroanal. Chem. Interfacial Electrochem. 248 (1988) 431–440, https://doi.org/10.1016/0022-0728(88)85103-9.

[32] R. Sabatini, T. Gorni, S. De Gironcoli, Nonlocal van der Waals density functional made simple and efficient, Phys. Rev. B - Condens. Matter Mater. Phys. 87 (2013), 041108, https://doi.org/10.1103/PHYSREVB.87.041108/FIGURES/3/MEDIUM.

[33] J. Enkovaara, C. Rostgaard, J.J. Mortensen, J. Chen, M. Dułak, L. Ferrighi, J. Gavnholt, C. Glinsvad, V. Haikola, H.A. Hansen, H.H. Kristoffersen, M. Kuisma, A.H. Larsen, L. Lehtovaara, M. Ljungberg, O. Lopez-Acevedo, P.G. Moses, J. Ojanen, T. Olsen, V. Petzold, N.A. Romero, J. Stausholm-Møller, M. Strange, G. A. Tritsaris, M. Vanin, M. Walter, B. Hammer, H. Häkkinen, G.K.H. Madsen, R. M. Nieminen, J.K. Nørskov, M. Puska, T.T. Rantala, J. Schiøtz, K.S. Thygesen, K. W. Jacobsen, Electronic structure calculations with GPAW: a real-space implementation of the projectoraugmented-wave method, J. Phys. Condens. Matter. 22 (25) (2010), 253202, https://doi.org/10.1088/0953-8984/22/25/253202.

[34] A. Held, M. Walter, Simplified continuum solvent model with a smooth cavity based on volumetric data, J. Chem. Phys. 141 (17) (2014), 174108, https://doi.org/10.1063/1.4900838.

[35] R.L. Gardas, M.G. Freire, P.J. Carvalho, I.M. Marrucho, I.M.A. Fonseca, A.G. M. Ferreira, J.A.P. Coutinho, PρT measurements of imidazolium-based ionic liquids, J. Chem. Eng. Data. 52 (2007) 1881–1888, https://doi.org/10.1021/JE700205N.

[36] S. Lysgaard, No Title, (n.d.). https://doi.org/10.11583/DTU.22617004.

[37] A.A. Peterson, Global optimization of adsorbate-surface structures while preserving molecular identity, Top. Catal. 57 (2014) 40–53, https://doi.org/10.1007/S11244-013-0161-8/FIGURES/10.

[38] G. Henkelman, H. Jónsson, Improved tangent estimate in the nudged elastic band method for finding minimum energy paths and saddle points, Aip. Scitation. Org. 113 (22) (2000) 9978–9985.

[39] A. Hjorth Larsen, J. Jørgen Mortensen, J. Blomqvist, I.E. Castelli, R. Christensen, M. Dułak, J. Friis, M.N. Groves, B. Hammer, C. Hargus, E.D. Hermes, P.C. Jennings, P. Bjerre Jensen, J. Kermode, J.R. Kitchin, E. Leonhard Kolsbjerg, J. Kubal, K. Kaasbjerg, S. Lysgaard, J. Bergmann Maronsson, T. Maxson, T. Olsen, L. Pastewka, A. Peterson, C. Rostgaard, J. Schiøtz, O. Schütt, M. Strange, K. S. Thygesen, T. Vegge, L. Vilhelmsen, M. Walter, Z. Zeng, K.W. Jacobsen, The atomic simulation environment—a python library for working with atoms, J. Phys. Condens. Matter. 29 (27) (2017), 273002, https://doi.org/10.1088/1361-648X/AA680E.

[40] W.A. Appiah, D. Kim, J. Song, M.-H. Ryou, Y.M. Lee, Understanding the effect of polydopamine interlayer on the long-term cycling performance of silicon anodes: a multiphysics-based model study, Batter. Supercaps. 2 (6) (2019) 541–550.

[41] Q.i. Zhang, R.E. White, Capacity fade analysis of a lithium ion cell, J. Power Sources. 179 (2) (2008) 793–798.

[42] W.A. Appiah, M.-H. Ryou, Y.M. Lee, A physics-based model capacity fade analysis of LiMn<inf>2</inf>O<inf>4</inf>/graphite cell at different temperatures, J. Electrochem. Soc. 166 (2019), https://doi.org/10.1149/2.0161903jes.

[43] P. Altimari, F. Greco, F. Pagnanelli, Nucleation and growth of metal nanoparticles on a planar electrode: A new model based on iso-nucleation-time classes of particles, Electrochim. Acta. 296 (2019) 82–93, https://doi.org/10.1016/J.ELECTACTA.2018.10.198.

[44] Y. Yuan, G. Luo, N. Li, New in situ description of electrodepositing multiple nucleation processes under galvanostatic stimuli, RSC Adv. 11 (2021) 31526–31532, https://doi.org/10.1039/D1RA04988G.

[45] G. Yue, S. Zhang, Y. Zhu, X. Lu, S. Li, Z. Li, A promising method for electrodeposition of aluminium on stainless steel in ionic liquid, AIChE J. 55 (2009) 783–796, https://doi.org/10.1002/AIC.11698.

[46] D. Pradhan, R.G. Reddy, Mechanistic study of Al electrodeposition from EMIC–AlCl3 and BMIC–AlCl3 electrolytes at low temperature, Mater. Chem. Phys. 143 (2014) 564–569, https://doi.org/10.1016/J.MATCHEMPHYS.2013.09.033.

[47] C. Lv, X. Zhou, L. Zhong, C. Yan, M. Srinivasan, W. Seh, C. Liu, H. Pan, S. Li, Y. Wen, Q. Yan, C. Lv, L. Zhong, C. Yan, M. Srinivasan, S. Li, Q. Yan, X. Zhou, Y. Wen, Z.W. Seh, C. Liu, H. Pan, Machine learning: an advanced platform for materials development and state prediction in lithium-ion batteries, Adv. Mater. 34 (2022) 2101474, https://doi.org/10.1002/ADMA.202101474.

[48] W.A. Appiah, J. Busk, T. Vegge, A. Bhowmik, Sensitivity analysis methodology for battery degradation models, Electrochim. Acta. 439 (2023), 141430, https://doi.org/10.1016/J.ELECTACTA.2022.141430.